ARMA 18–879

Development and Testing of Advanced Inter-Well Pressure Pulse Analysis for Fracture Diagnostics in Tight Gas Reservoirs

Ramos, J., Wang, W., Bruno, M.S., Lao, K. and Oliver, N.
GeoMechanics Technologies, Monrovia, California, United States of America

This paper was prepared for presentation at the 52nd US Rock Mechanics / Geomechanics Symposium held in Seattle, Washington, USA, 17–20 June 2018. This paper was selected for presentation at the symposium by an ARMA Technical Program Committee based on a technical and critical review of the paper by a minimum of two technical reviewers. The material, as presented, does not necessarily reflect any position of ARMA, its officers, or members. Electronic reproduction, distribution, or storage of any part of this paper for commercial purposes without the written consent of ARMA is prohibited. Permission to reproduce in print is restricted to an abstract of not more than 200 words; illustrations may not be copied. The abstract must contain conspicuous acknowledgement of where and by whom the paper was presented.

ABSTRACT: Unconventional gas reservoirs constitute a major component of U. S. gas production. Tight gas reservoirs are an important part of this unconventional gas production. The common completion technique for horizontal wells in shale gas reservoirs is hydraulic fracturing in multi-stages. A novel technique was developed to monitor and characterize hydraulic fractures through the analysis of pressure pulse data recorded at offset wells before, during, and after horizontal well fracture operations in tight gas reservoirs. Two methodologies were defined and tested to characterize fracture orientation for single vertical fractures. The first methodology encompasses pressure pulse response before and after hydraulic fracturing, and the second involves using type curves that match a pressure pulse response after an existing hydraulic fracture was created. Based on the analytical and numerical results, preliminary families of type curves were generated for different well pair spacing and orientation of the fracture plane. Field data was applied for calibration and validation and an inversion technique was used to match the numerical results with field observations. Results indicated a successful fracture characterization with a reasonable cost-effective technique correlation between the numerical model and the field case.

1. INTRODUCTION

Unconventional gas reservoirs constitute a major component of U. S. gas production. Tight gas reservoirs are an important part of this unconventional gas production. The common completion technique for horizontal wells in shale gas reservoirs is hydraulic fracturing in multi-stages. With increased application of fracturing in horizontal wells, it is critical to better characterize the fracture geometry and orientation both to optimize production and at the same time to ensure fracture containment in the target interval to avoid out of zone gas migration.

Fracture diagnostic techniques include direct and indirect techniques. The most well-known direct technique is microseismic fracture mapping and tiltmeter fracture mapping. These techniques require sophisticated instrumentation embedded in boreholes surrounding the well to be fracture treated. Although direct far-field techniques can be used to map hydraulic fractures, the technology is still under development. Furthermore, direct techniques are expensive and time consuming. Indirect fracture mapping techniques consist of hydraulic fracture numerical modelling of net pressure, pressure transient test analyses, and production data analyses. Indirect fracture diagnostic techniques are most widely used to determine the shape and dimension of the created fracture, however, the solution from most of the current indirect techniques may not be unique and may require as much fixed data as possible.

Well test analysis involves generating and measuring pressure variations with time in the well in order to estimate rock, fluid, and well properties. Well testing is considered essential in many phases of petroleum engineering. Information from these tests helps reservoir engineers analyze reservoir performance and predict future production under different operational mechanisms. Well tests including interference and pulse tests have been used to evaluate the vertical fracture geometry and orientation over the past decades (Brigham, 1969; Kamal and Brigham, 1974; Pierce et al., 1974; Ekie et al., 1977; Earlougher, 1979; Kamal, 1982; El-Khatib, 2011; El-Khatib, 2013).

Current analytical solutions from interference and pulse testing are limited in application due to necessary simplifying assumptions, although they represent a key and important first step for understanding physical behavior and the relative importance of various parameters. For example, most analytical equations for geomechanics and fluid flow problems require assumptions of formation homogeneity and isotropy, simple geometric shapes for fractures and reservoirs, and flat two-dimensional infinite acting reservoirs without complex structures or boundaries. These assumptions are

rarely valid for real world oil and gas reservoirs and well configurations. In general, therefore, numerical (computer) models must be applied to take into account more complex (and realistic) situations.

The objective of this research is to develop and demonstrate with field data a more accurate and cost-effective technique to estimate fracture height, length, and orientation than currently available technology. We propose to develop advanced techniques to analyze pressure pulses from horizontal well fracture operations recorded at offset wells or at other perforation/stage locations within the same well to monitor and characterize hydraulic fractures. Variable reservoir conditions can be considered accounting for dipping and varying lithology. Finally, the developed technique is compared and calibrated against actual field data from fracture operations, in which pressure sensors were placed at multiple offset well locations.

2. REVIEW OF PRESSURE PULSE TESTING

2.1. Pulse Testing Theory and Terminology

A conventional pulse test can be defined as a series of flow disturbances generated at one well referred to as the "pulsing well" and the pressure is recorded in another well referred to as the "observation/monitoring well". These disturbances at the pulsing well are generated by alternating either injection and shut-in periods or production and shut-in periods. At the observation well, a sensitive differential pressure gauge records the pressure response, including timing and amplitude. A typical pulse test configuration example is presented in Fig. 1.

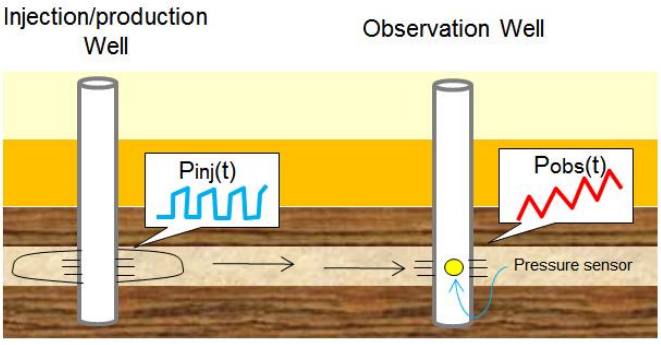

Fig. 1. Typical pulse test configuration example.

The pressure response at the observation well is usually quite small, sometimes less than 68 Pa (0.01 psi). Therefore, very sensitive pressure measuring equipment is required. The major advantage of a pulse test versus a conventional interference test are (1) the cyclical nature of the pressure response at the observation well can more easily be distinguished from the background pressure response, and (2) it is shorter in duration, lasting from a few hours to a few days compared to weeks and months for a conventional interference test. A complete description of the procedure and terminology of pulse testing has been presented in the past by Johnson et al., 1966.

Two characteristics of pressure response at the observation well are used for conducting a pulse test analysis. One is the time lag (t_{L1}, t_{L2},…), the time between the end of a pulse and the pressure peak caused by the pulse. The second is the amplitude of the pressure response (Δp_1, Δp_2,…) usually measured between two parallel tangent lines. Fig. 2 shows the time lags and pressure response amplitudes for a hypothetical pulse test. Pulse amplitude depends on flow rate, pulse interval, reservoir properties, transmissibility, and storage.

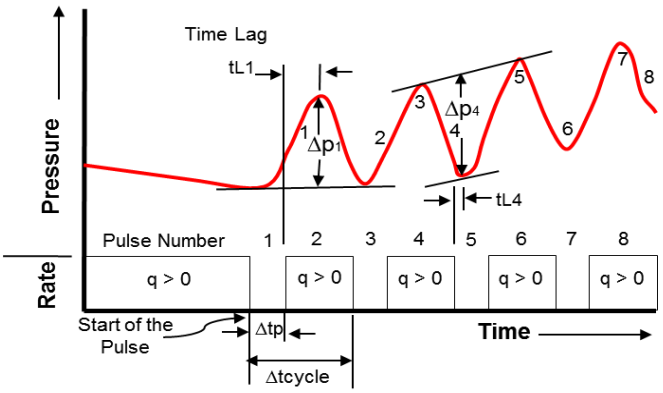

Fig. 2. Pulse test rate and pressure history showing the definition of time lag and pulse response amplitude (After Ahmed and McKinney, 2005).

It has been shown that the presence of a high-transmissibility zone or of a zone of very low transmissibility can be detected by pulse testing (Vela et al., 1969). A fracture creates a zone of high transmissibility with an insignificant change in storage as compared with that of the unfractured matrix. A change in time lag is sensitive to a change in transmissibility. However, pulse amplitude varies directly with changes in transmissibility as described by Pierce, et al., 1974. Thus, changes in time lag should be most effective for determining the direction and length of a hydraulic fracture.

The mathematical model for a uniform-flux fracture has been discussed by Gringarten et al., 1972 and Uraiet et al., 1977 and was used to illustrate the pulse theory. Assume that a single vertical fracture intersects a wellbore located in an infinite, homogeneous, porous medium. The surface production rate is assumed constant and all the production is obtained by means of the fracture. Fluid enters the fracture at the same rate per unit area of the fracture (uniform-flux fracture). As

shown by Gringarten et al., 1972, the pressure distribution surrounding this fracture is given by:

$$P_D(x_d, y_d, t_d) = \frac{\sqrt{\pi}}{4}\int_0^{td} exp\left(-{y_D}^2/4\tau_D\right)\left[erf\frac{(1-x_D)}{2\sqrt{\tau_D}} + erf\frac{(1+x_D)}{2\sqrt{\tau_D}}\right]\frac{d_{\tau_D}}{\sqrt{\tau_D}} \quad (1)$$

where

$$P_D(x_d, y_d, t_d) = \frac{kh}{141.2qB\mu}\left[p_i - p(x, y, t)\right] \quad (2)$$

$$t_D = \frac{0.000264kt}{\phi C_t \mu {x_f}^2} \quad (3)$$

$$x_D = \frac{x}{x_f} \quad (4)$$

$$y_D = \frac{y}{x_f} \quad (5)$$

Here, P_D (x_D, y_D, t_D) is the dimensionless pressure drop and t_D is the dimensionless time based on the fracture half-length, xf. Dimensionless distances x_D and y_D are also based on the fracture half-length. Eq. (2) and Eq. (3) are in oilfield units.

2.2. Analytical Methods for Pulse Testing Analysis

Pierce et al., 1974 proposed a method to detect both the fracture orientation and length from pulse testing. This method involves pulse testing a given well before and after fracturing. The response at several adjacent wells is measured in both tests and a plot of the ratio between the time lag before fracturing and the time lag after fracturing vs. the angle between the line connecting the two wells and the due-North line was developed. This plot will have a "W" shape and the fracture orientation is the angle at which the peak occurs.

When the pressure response is monitored through unequal radial distance between pulsing well and observation wells, the time lag before and after fracture ratio should be corrected by:

$$\left(\frac{t_{LB}}{t_{LA}}\right)^{-\frac{1}{2}}_{corr} - 1 = \left[\left(\frac{t_{LB}}{t_{LA}}\right)^{-\frac{1}{2}} - 1\right] * \frac{r}{r_{min}} \quad (6)$$

where, t_{LB}, t_{LA} are the time lag before and after fracture, r is the radial distance between pulse and response well and r_{min} is the minimum radial distance between pulse and response well.

Fig. 3 shows an example of detecting the fracture orientation using the W shape – at 180 degree from North. Note that the sensitivity of this method decreases with the ratio of the fracture length (L_f) to the distance between the wells (r). The disadvantage of this method is that this method requires both pre-fracture and post-fracture data.

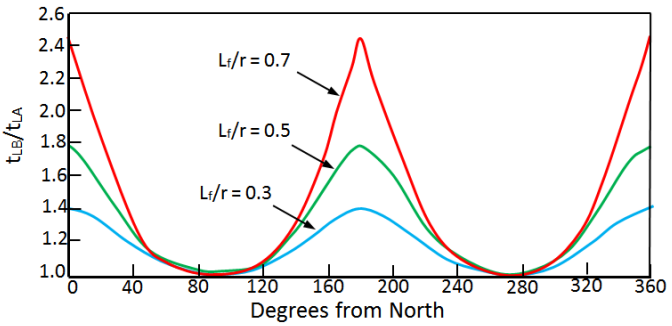

Fig. 3. "W" shape curve example. Relation of angle and fracture length to time lag before and after fracture (After Pierce et al., 1974).

Uraiet et al., 1977 used the uniform-flux fracture model and generated type curves for interference tests. These curves relate the dimensionless pressure drop to the ratio of dimensionless time and dimensionless wellbore radius for several angles between the fracture orientation and the line connecting the two wells. They found that the test results are more sensitive to the fracture orientation (θ) for θ < 45°. To apply this technique, at least two observation wells are required to determine the fracture orientation. Cinco-Ley and Samaniego, 1977 extended the work of Uraiet et al., 1977 to finite-conductivity fractures.

Ekie et al., 1977 also used the uniform-flux fracture model to test the effect of fracture orientation on pulse tests. They generated correlation curves for each value of dimensionless radius and pulse ratio and described how the fracture orientation can be determined by these curves if the formation permeability and/or fracture length are known. The dimensionless time lag (t_{lD}), dimensionless cycle period (Δt_{cycD}) and dimensionless distance (r_D) were defined respectively by:

$$\boldsymbol{tl_D = \frac{tl}{\Delta t_{cyc}}} \quad (7)$$

$$\boldsymbol{\Delta t_{cycD} = \frac{0.000264 * k * \Delta t_{cyc}}{\emptyset * ct * \mu * r^2}} \quad (8)$$

$$\boldsymbol{r_D = \frac{r}{Xf}} \quad (9)$$

where *tl* is the time lag, Δt_{cyc} is the cycle period, *k* is the permeability, ϕ is the porosity, *ct* is the total rock compressibility, μ is the viscosity, *r* is the radial distance between the pulsing and responding well, and x_f is the fracture half-length.

3. PRESSURE PULSE MODEL DEVELOPMENT

3.1. Numerical Model Development

Numerical modeling allows for the evaluation of pressure response at different reservoir conditions during pulse testing while testing the sensitivity of operational parameters. Combined with the analytical solution, it can lead to a better understanding of pressure response and therefore, a better approach for fracture characterization.

A conceptual model was assembled with a mesh covering an area of 1600x1600x30 m (5249x5249x98 ft) at a depth of 3000 m (9842.51 ft) as can be seen in Fig. 4. Constant reservoir pressure was assumed as a lateral boundary condition and no flow conditions were assigned to the top and bottom. A fracture oriented from North to South (0 degrees) and a pulsing well was added in the middle of the model to evaluate pressure response at the observation wells. A mesh with higher refined elements at the central area was defined along the x-axis, followed by two zones with less refined elements outside of the refinement zone. A similar condition was defined along the y-axis. Along the z-axis, three elements were considered to represent the reservoir thickness of 30 m (98.4 ft). Fig. 5 shows the conceptual mesh for the numerical model.

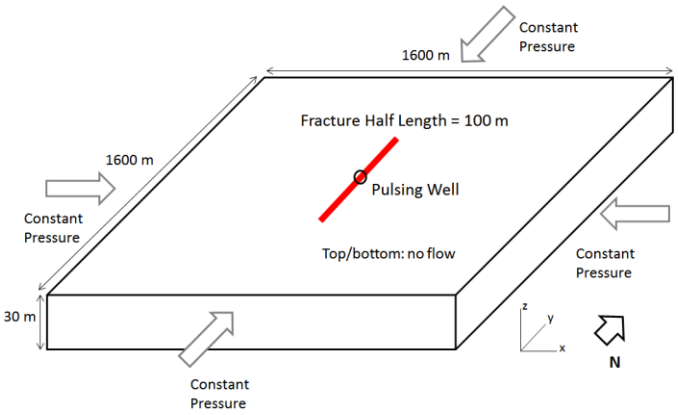

Fig. 4. Conceptual model for numerical simulation.

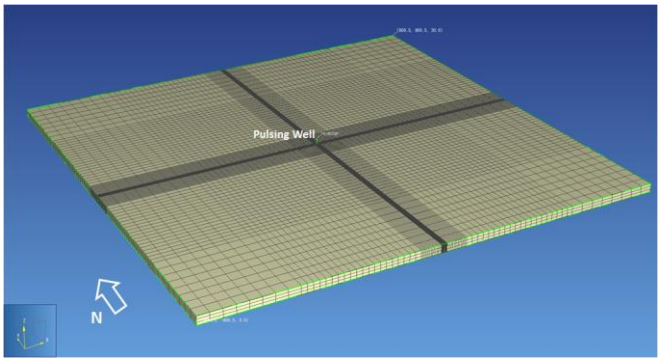

Fig. 5. Conceptual mesh for numerical simulation.

Reservoir and fluid flow properties considered on the conceptual numerical simulation are summarized in Table 1.

Table 1. Reservoir and fluid flow data for numerical simulation.

Parameters		Values
Reservoir	Permeability	0.1 mD
	Porosity	0.15
	Thickness	30 m (98.4 ft)
Fracture	Permeability	1000 mD
	Porosity	0.1
	Half Length	100 m (328 ft)
Injection rate		1.5 m^3/min (400 gpm)

3.2. Case 1: Pressure Response Analysis Before and After Hydraulic Fracturing

To analyze the pressure pulse response before and after the hydraulic fracturing, Pierce's method was applied considering observation wells at different angles and radial distances from the pulsing well. A total of seven well pair combinations were evaluated as seen in Fig. 6.

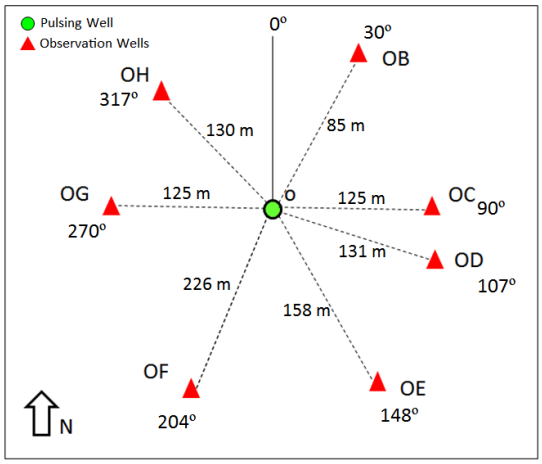

Fig. 6. Observation well distribution surrounding the pulsing well for Case 1 analysis.

For the Case 1 analysis, pressure response was evaluated prior the fracture for an injection period of 10 hours at a constant rate of 1.5 m^3/min (400 gpm), followed by a shut-in period of 10 hours until a cycle period was conducted (Fig. 7). Time lag was estimated as the difference between the maximum pressure response value and the total injection time of 10 hours for each well pair as shown in Fig. 8. Note that the pressure response is referenced on the left y-axis and the injection pressure at the pulsing well on the right y-axis.

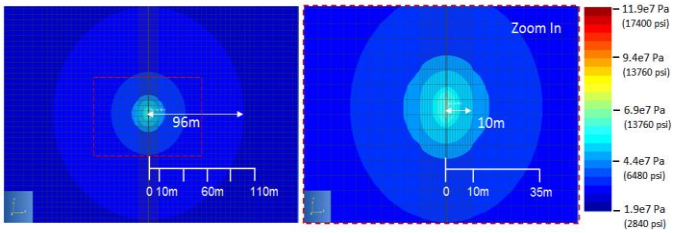

Fig. 7. Top view of pressure distribution (left) and zoom in (right) after 10 hours of injection before hydraulic fracture for the Case 1 analysis.

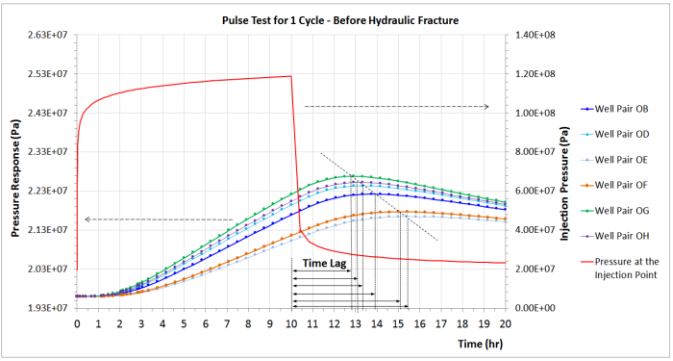

Fig. 8. Pressure response before the hydraulic fracture at different well pairs.

As seen in Fig. 8, the pressure response is affected by the distance between the active well and the observation well, as well as the angle from the north. In this case, the maximum pressure response of 2.26e7 Pa (3290 psi) with a time lag approximately of 2.92 hr was obtained for well pair OG and the minimum pressure response of 2.16e7 Pa (3140 psi) with a time lag approximately of 5.42 hr was obtained for well pair OE. Because well pair OE is farther (158 m) from the injection point, it takes more time for the pressure response and therefore, a higher time lag was experienced.

The pressure response after the hydraulic fracture takes place is illustrated in Fig. 9. As shown, a similar pressure response occurs with the well pair OE that is far from the injection point with the higher time lag of 4.58 hr. By comparing both results presented in Fig. 8 and Fig. 9, the presence of the fracture leads to a reduction on the time lag because the fluid reaches faster to each monitoring well.

The ratio of the time lag before and after the hydraulic fracture was estimated. Based on Pierce's method, and because of the radial distance between each well pair is different, the time lag ratio was corrected by Eq. (6). The ratio is fixed as a function of the minimum radial distance, which is 85 m (278 ft) for well pair OB. This equation was solved numerically by Newton-Raphson's method to find the best root approximation. Table 2 summarizes the time lag results corrected for each well pair.

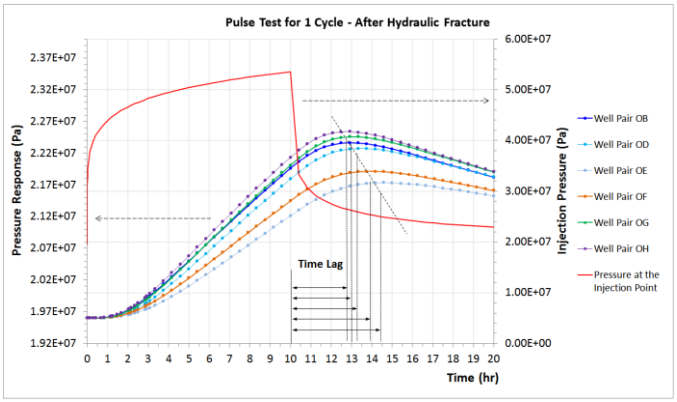

Fig. 9. Pressure response after the hydraulic fracture at different well pairs.

Table 2. Time lag before and after the fracture for each well pair.

Well Pair	Angle from North (°)	r (m)	t_{LB} (hr)	t_{LA} (hr)	t_{LB}/t_{LA}	t_{LB}/t_{LA} Corrected
OB	30	85	3.75	2.92	1.29	1.29
OC	90	125	2.92	2.92	1.00	1.00
OD	107	131	3.33	3.33	1.00	1.00
OE	148	158	5.42	4.58	1.18	1.38
OF	204	226	4.32	3.75	1.15	1.49
OG	270	125	2.92	2.92	1.00	1.00
OH	317	130	3.33	2.92	1.14	1.23

To estimate the potential fracture orientation, we plotted the time lag ratio vs. the angle from the north for each well pair. The analysis was conducted by grouping the results of the well pairs on the west and east of the pulsing well. Based on this, two trendlines with their respective forecast polynomial equations were estimated at both sides of the fracture (left and right). A W-shape curve was defined by combining both trendline results (Fig. 10). In theory, the peak of the curve with the higher values corresponds to the fracture orientation that matches the pre-defined orientation at zero degrees from north (equivalent to 180 degrees).

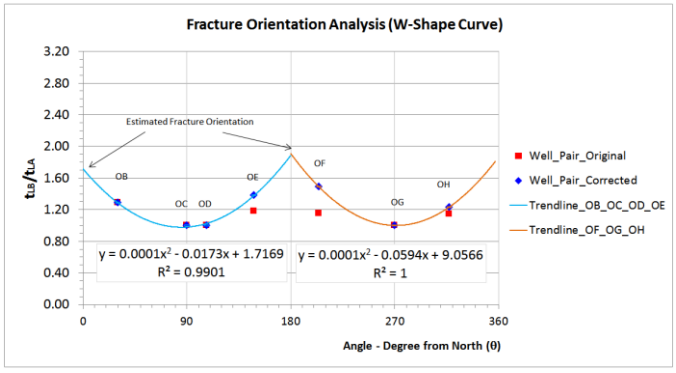

Fig. 10. W-shape curve for fracture orientation analysis.

3.3. *Case 2: Pressure Response Analysis After Hydraulic Fracturing*

This analysis only involves the pulse pressure response for post-fracturing. To conduct this analytical solution method, a data set of pressure responses derived from numerical simulation was taken into account at different fracture orientations and radial distances to create different families of type curves. Because the model is symmetric, a single quarter was only used for pressure response analysis to create the database and estimate the type curves. Fig. 11 presents a quarter of the model with the observation wells shown.

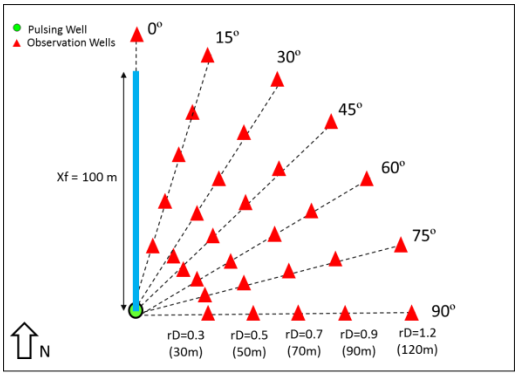

Fig. 11. Observation wells distribution surrounding the pulsing well for the Case 2 analysis.

A family of type curves was defined for each dimensionless distance (r_D) at different fracture orientation angles while varying the pulse cycle period. In this case, to simplify the model, we assumed the pulse periods and the shut-in periods to be the same duration as shown in Table 3. In addition, two cycle periods were considered to calculate the time lag using the tangent method in the first even pulse response as defined by Ekie et al., 1977. Then, applying Eq. (7) and Eq. (8), a database of dimensionless time lag and dimensionless cycle periods was created. Table 4 and Table 5 show the database for an r_D of 0.7 and r_D of 1.2 respectively, varying the orientation angle from the north.

Table 3. Pulse cycles periods. Equal time for pulsing and shut-in was modeled to simplify the model.

Pulse Cycles Periods
1hr Pulse - 1hr Shut-in
2hr Pulse - 2hr Shut-in
5hr Pulse - 5hr Shut-in
10hr Pulse - 10hr Shut-in
14hr Pulse - 14hr Shut-in
20hr Pulse - 20hr Shut-in
30hr Pulse - 30hr Shut-in

Table 4. Dimensionless time lag and dimensionless cycle periods for an r_D=0.7.

Angle from North (°)	Pulse Cycle Period	t_L (hr)	ΔT_Cycle (hr)	t_{LD}	ΔT_CycleD
90	0.5h Pulse - 0.5h Shut-in	0.45	1.00	0.45	21.25
	1h Pulse - 1h Shut-in	0.65	2.00	0.33	42.49
	2h Pulse - 2h Shut-in	0.75	4.00	0.19	84.98
	5h Pulse - 5h Shut-in	0.44	10.00	0.04	212.45
	10h Pulse - 10h Shut-in	0.29	20.00	0.01	424.91
	14h Pulse - 14h Shut-in	0.24	28.00	0.009	594.87
75	0.5h Pulse - 0.5h Shut-in	0.44	1.00	0.44	21.25
	1h Pulse - 1h Shut-in	0.64	2.00	0.32	42.49
	2h Pulse - 2h Shut-in	0.73	4.00	0.18	84.98
	5h Pulse - 5h Shut-in	0.4	10.00	0.04	212.45
	10h Pulse - 10h Shut-in	0.25	20.00	0.01	424.91
	14h Pulse - 14h Shut-in	0.22	28.00	0.01	594.87
60	0.5h Pulse - 0.5h Shut-in	0.42	1.00	0.42	21.25
	1h Pulse - 1h Shut-in	0.59	2.00	0.30	42.49
	2h Pulse - 2h Shut-in	0.60	4.00	0.15	84.98
	5h Pulse - 5h Shut-in	0.30	10.00	0.03	212.45
	10h Pulse - 10h Shut-in	0.20	20.00	0.01	424.91
	14h Pulse - 14h Shut-in	0.18	28.00	0.01	594.87
45	0.5h Pulse - 0.5h Shut-in	0.39	1.00	0.390	21.25
	1h Pulse - 1h Shut-in	0.53	2.00	0.265	42.49
	2h Pulse - 2h Shut-in	0.48	4.00	0.120	84.98
	5h Pulse - 5h Shut-in	0.25	10.00	0.025	212.45
	10h Pulse - 10h Shut-in	0.17	20.00	0.009	424.91
	14h Pulse - 14h Shut-in	0.15	28.00	0.005	594.87
30	0.5h Pulse - 0.5h Shut-in	0.36	1.00	0.36	21.25
	1h Pulse - 1h Shut-in	0.47	2.00	0.24	42.49
	2h Pulse - 2h Shut-in	0.4	4.00	0.10	84.98
	5h Pulse - 5h Shut-in	0.21	10.00	0.02	212.45
	10h Pulse - 10h Shut-in	0.15	20.00	0.01	424.91
	14h Pulse - 14h Shut-in	0.13	28.00	0.00	594.87
15	0.5h Pulse - 0.5h Shut-in	0.29	1.00	0.29	21.25
	1h Pulse - 1h Shut-in	0.36	2.00	0.18	42.49
	2h Pulse - 2h Shut-in	0.3	4.00	0.08	84.98
	5h Pulse - 5h Shut-in	0.16	10.00	0.02	212.45
	10h Pulse - 10h Shut-in	0.12	20.00	0.01	424.91
	14h Pulse - 14h Shut-in	0.10	28.00	0.00	594.87

Table 5. Dimensionless time lag and dimensionless cycle periods for an r_D=1.2.

Angle from North (°)	Pulse Cycle Period	t_L (hr)	ΔT_Cycle (hr)	t_{LD}	ΔT_CycleD
90	1h Pulse - 1h Shut-in	1.10	2.00	0.55	14.46
	2h Pulse - 2h Shut-in	1.70	4.00	0.43	28.92
	5h Pulse - 5h Shut-in	2.25	10.00	0.23	72.29
	10h Pulse - 10h Shut-in	2.00	20.00	0.10	144.59
	14h Pulse - 14h Shut-in	1.75	28.00	0.06	202.42
	20h Pulse - 20h Shut-in	1.50	40.00	0.04	289.17
	30h Pulse - 30h Shut-in	1.20	60.00	0.02	433.76
75	1h Pulse - 1h Shut-in	1.06	2.00	0.53	14.46
	2h Pulse - 2h Shut-in	1.64	4.00	0.41	28.92
	5h Pulse - 5h Shut-in	2.2	10.00	0.22	72.29
	10h Pulse - 10h Shut-in	1.95	20.00	0.10	144.59
	14h Pulse - 14h Shut-in	1.65	28.00	0.06	202.42
	20h Pulse - 20h Shut-in	1.41	40.00	0.04	289.17
	30h Pulse - 30h Shut-in	1.13	60.00	0.02	433.76
60	1h Pulse - 1h Shut-in	0.98	2.00	0.49	14.46
	2h Pulse - 2h Shut-in	1.54	4.00	0.39	28.92
	5h Pulse - 5h Shut-in	2.06	10.00	0.21	72.29
	10h Pulse - 10h Shut-in	1.74	20.00	0.09	144.59
	14h Pulse - 14h Shut-in	1.48	28.00	0.05	202.42
	20h Pulse - 20h Shut-in	1.20	40.00	0.03	289.17
45	1h Pulse - 1h Shut-in	0.92	2.00	0.46	14.46
	2h Pulse - 2h Shut-in	1.46	4.00	0.37	28.92
	5h Pulse - 5h Shut-in	1.94	10.00	0.19	72.29
	10h Pulse - 10h Shut-in	1.57	20.00	0.08	144.59
	14h Pulse - 14h Shut-in	1.20	28.00	0.04	202.42
	20h Pulse - 20h Shut-in	0.96	40.00	0.02	289.17
30	1h Pulse - 1h Shut-in	0.87	2.00	0.44	14.46
	2h Pulse - 2h Shut-in	1.36	4.00	0.34	28.92
	5h Pulse - 5h Shut-in	1.72	10.00	0.17	72.29
	10h Pulse - 10h Shut-in	1.31	20.00	0.07	144.59
	14h Pulse - 14h Shut-in	0.99	28.00	0.04	202.42
	20h Pulse - 20h Shut-in	0.71	40.00	0.02	289.17
15	1h Pulse - 1h Shut-in	0.78	2.00	0.39	14.46
	2h Pulse - 2h Shut-in	1.20	4.00	0.30	28.92
	5h Pulse - 5h Shut-in	1.25	10.00	0.13	72.29
	10h Pulse - 10h Shut-in	1.00	20.00	0.05	144.59
	14h Pulse - 14h Shut-in	0.7	28.00	0.03	202.42
	20h Pulse - 20h Shut-in	0.60	40.00	0.02	289.17
0	1h Pulse - 1h Shut-in	0.65	2.00	0.33	14.46
	2h Pulse - 2h Shut-in	0.90	4.00	0.23	28.92
	5h Pulse - 5h Shut-in	0.87	10.00	0.09	72.29
	10h Pulse - 10h Shut-in	0.60	20.00	0.03	144.59
	14h Pulse - 14h Shut-in	0.45	28.00	0.02	202.42
	20h Pulse - 20h Shut-in	0.10	40.00	0.00	289.17

Then, dimensionless time lag versus the product of dimensionless cycle period and dimensionless time lag was plotted, and a set of polynomial trendlines was predicted with the best trend/regression fit for each orientation angle. Fig. 12 and Fig. 13 show the result for an r_D of 0.7 and 1.2, respectively.

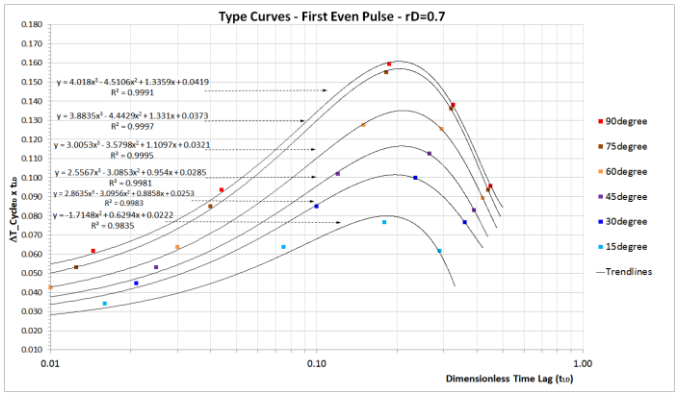

Fig. 12. Type curves for each orientation angle for a dimensionless distance of 0.7.

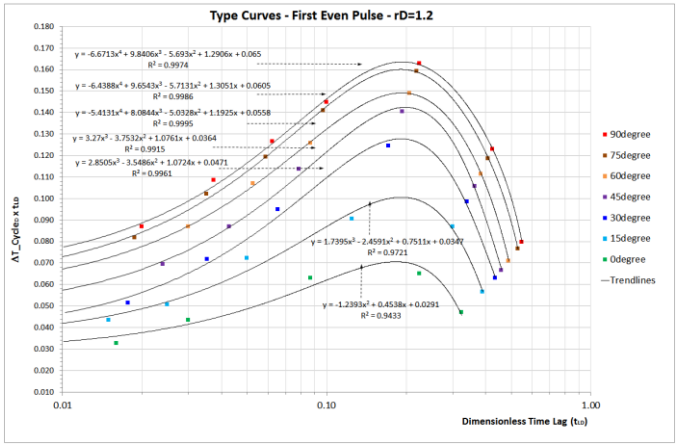

Fig. 13. Type curves for each orientation angle for a dimensionless distance of 1.2.

In addition, type curves comparison varying the dimensionless radial distance can be seen in Fig. 14. Note that a higher r_D leads to higher dimensionless time lag.

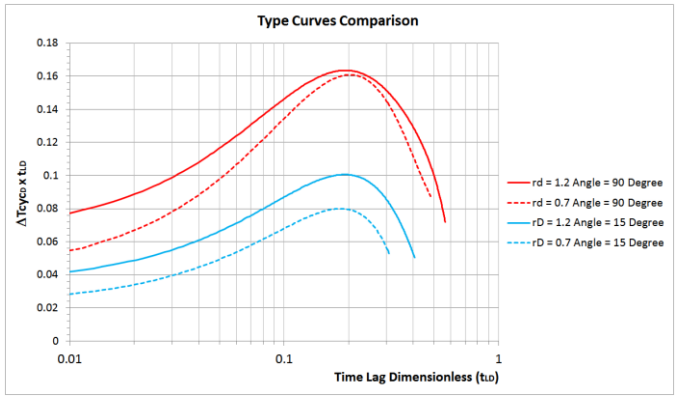

Fig. 14. Type curve comparison between r_D=0.7 and r_D=1.2.

4. FIELD DATA IMPLEMENTATION AND VALIDATION

4.1. Field Data Review

After conducting the theoretical review regarding pulse testing, as well as the analytical and numerical modeling, a field data validation was performed. To accomplish this, field conditions were simulated by numerical modeling and compared with real pressure response. Then, the orientation, length, and height of the fracture were defined using sensitivity analyses and matched with field data.

The data was collected from a couple of injection and observation wells from a field in southern California. In spite of the conceptual model was designed for a tight gas reservoir, the actual field data correspond to a conventional reservoir with 30 mD of permeability. A downhole bottom hole pressure (BHP) gauge in the monitoring well was deployed at 1426 m (4681 ft) from sub sea level as seen in Fig. 15 (left). It is also important to point out that the injection well is a vertical well and the observation well is slightly deviated up to 10 degrees from vertical and oriented at 30 degrees azimuth from north as presented in Fig. 15 (right).

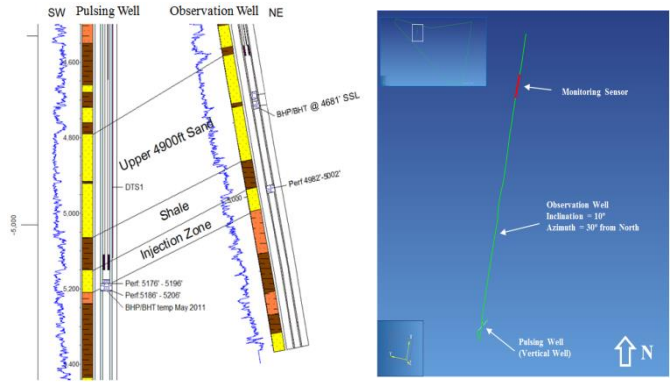

Fig. 15. NE-SW cross section (left) and top view well orientation (right) for pulsing and observation wells.

After reviewing the field data recorded from October 2015 to December 2015, a bottom hole pressure response period from December 21 to December 25 2015 was selected for the analysis as shown in Fig. 16. Moreover, a constant injection rate of 1.25 m^3/min (330 gpm) was maintained during the test. The analysis was conducted in the first and second cycles of the pulse testing.

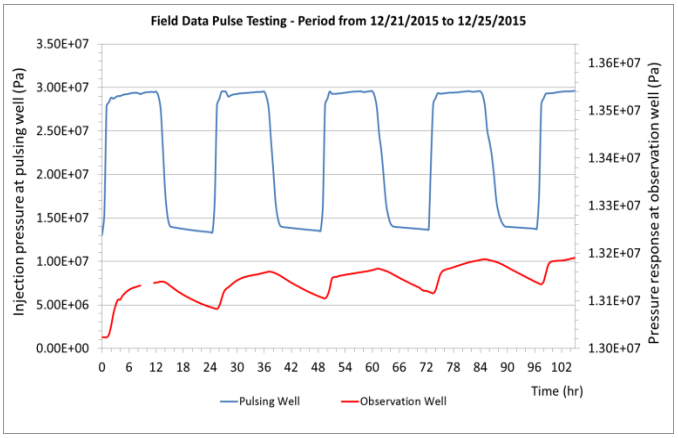

Fig. 16. Bottom hole pressure response at the injection and observation wells.

4.2. Numerical Fluid Flow Model with Field Conditions

A 3D fluid flow model was assembled in TOUGH2 around the area of interest as presented in Fig. 17. Note that the model is aligned with the strike of the sealing fault I at N65ºW.

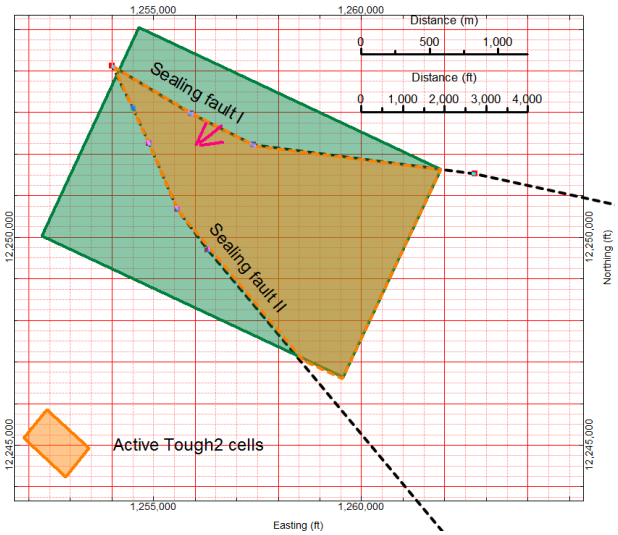

Fig. 17. Area covered by the 3D fluid flow model including the active cells.

The model was oriented at local coordinates as shown in Fig. 18. A 3D mesh geometry and the location of the wells are presented in Fig. 19. The mesh was refined in an area of 300 x 300 m (990 x 990 ft) with high resolution in the center where the wells are located.

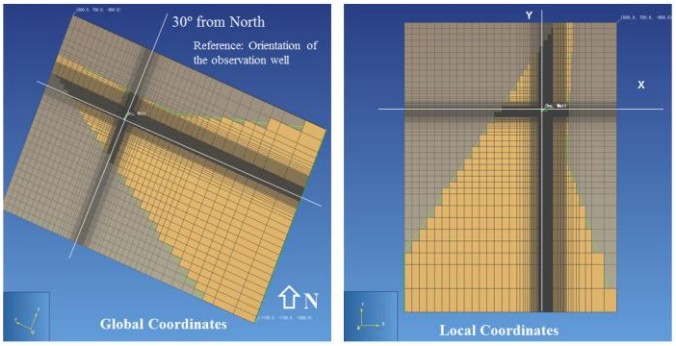

Fig. 18. Top view of global coordinates (left) and local coordinates (right) references for the fluid flow model.

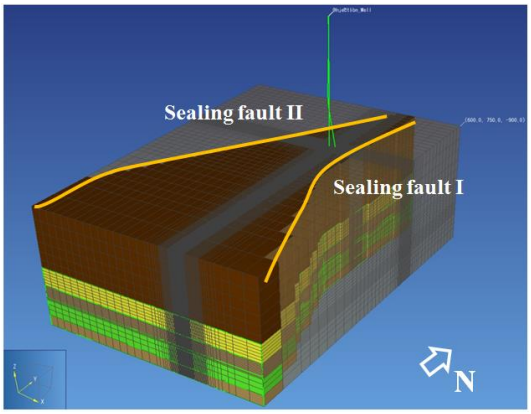

Fig. 19. 3D fluid flow model mesh. The boundaries of active cells were defined by the structural faults.

4.3. Sensitivity Analysis and Data Calibration

Due to the complexity of the reservoir, uncertainty in the fracture orientation, fracture geometry and permeability, sensitivity analyses were performed to calibrate the numerical results with the field data. Table 6 summarizes the sensitivity matrix with seven scenarios.

Table 6. Simulation matrix. A total of seven models were evaluated varying the fracture height and orientation.

Sensitivity	1	2	3	4	5	6	7
Fracture Height (m)	80	60	40	20	20	20	20
Fracture Orientation (degree)	0	0	0	0	45	70	90

Fracture height was the first sensitivity analysis conducted. A variation from 20 m to 80 m was considered as seen in Fig. 20. Overall, an increase in the fracture height influences the pressure response. In this case, higher fracture height decreases the pressure response. Note that a reasonable match with the actual field data was performed with a fracture height of 20 m (66 ft).

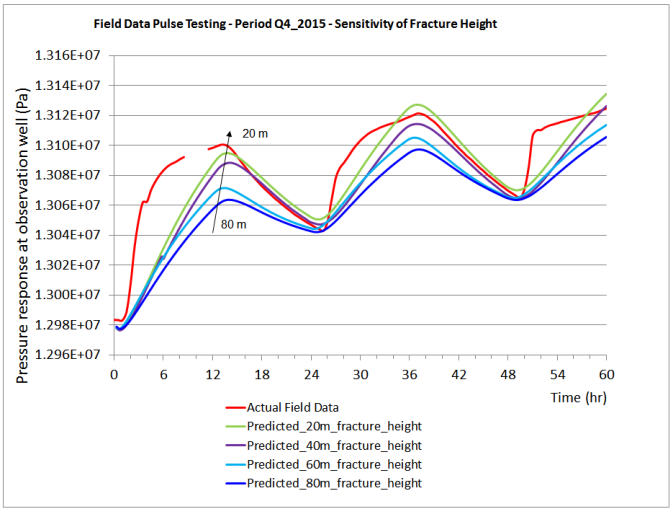

Fig. 20. Effect of fracture height on pressure response at the observation well.

Once the fracture height effect was analyzed, a variation of fracture orientation at 0º, 45º, 70º and 90º in the local coordinate xy plane was evaluated as shown in Fig. 21. Fig. 22 shows the fracture orientation sensitivity at 0º, 45º, 70º and 90º in the xy plane. As shown, the fracture oriented at 90º (plotted in a dash curve), presents a better match with the actual field data at the observation well represented by the red curve.

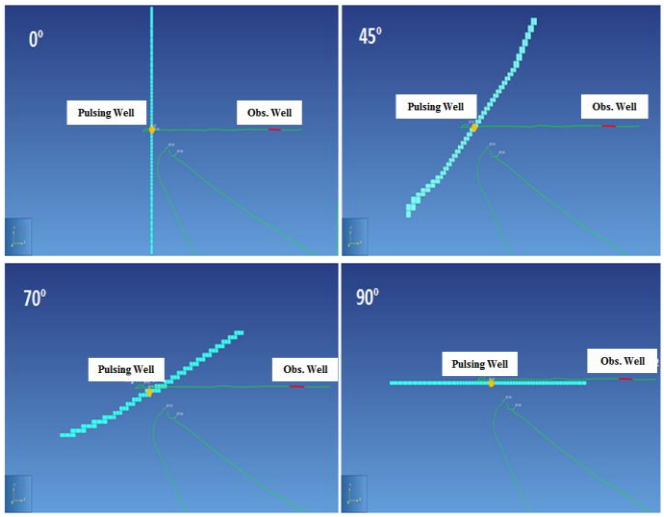

Fig. 21 Top view at the injection depth of 1574 m (5166 ft) showing the fracture orientation at 0º, 45º, 70º and 90º in the xy plane.

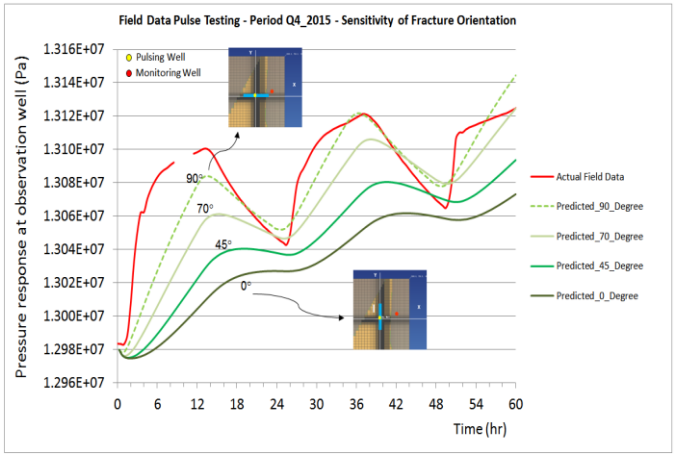

Fig. 22. Effect of fracture orientation on pressure response at the observation well.

After applying Ekie's method, a family of type curves for this area was generated and a comparison with the actual field data was presented in Fig. 23. Note that the field data is close to the 90º orientation curve. It is important to point out that this 90º is referred in a local coordinate system. Thus, the final fracture orientation in global coordinates is around 25º, which is almost parallel to the orientation of the observation well.

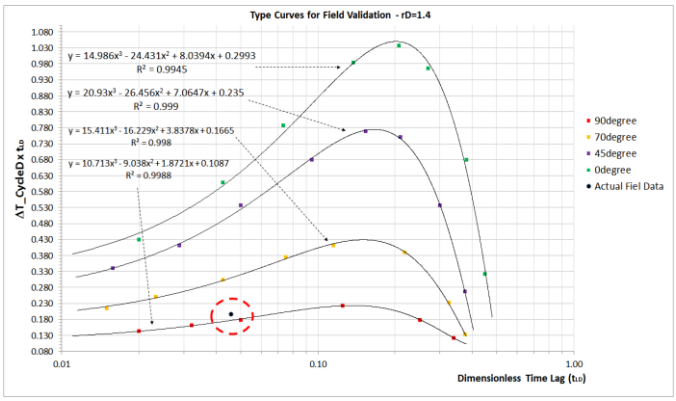

Fig. 23. Field type curves at a dimensionless distance of 1.4.

Finally, the results of the fracture orientation simulations were compared with the maximum horizontal stress orientation. Fig. 24 presents the maximum horizontal principal stress orientation obtained from the World Stress Map (World Stress Map, 2016).

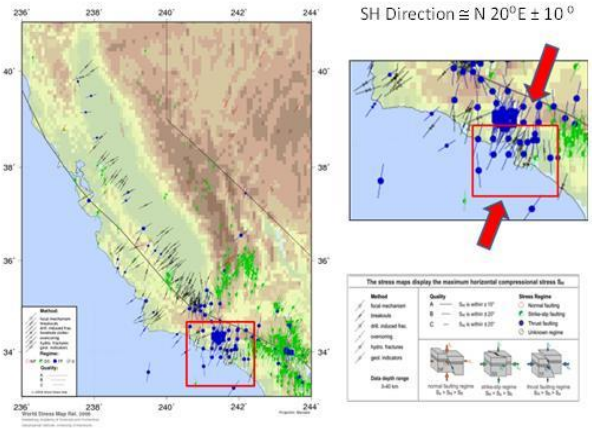

Fig. 24. Maximum horizontal principal stress orientation (After World Stress Map, 2016).

By comparing the maximum horizontal principal stress orientation of N20ºE±10º with the fracture orientation estimated of N25ºE, we can state that a reasonable match was determined with the analysis.

5. CONCLUSIONS

An advanced technique was developed to monitor and characterize hydraulic fractures by analyzing pressure pulse data for fracture operations recorded at offset wells or at other perforation/stage locations within the same well.

Analytical solutions and numerical models were implemented to evaluate single fractures from horizontal wells in a conceptual model with tight gas reservoir conditions. Two cases were defined and successfully tested. One case encompassed the pulse pressure response before and after the hydraulic fracture, and the second case involved pulse pressure response after an existing hydraulic fracture. For the first case, at minimum three monitoring points were required for an effective fracture characterization. However, for the second case, at least a minimum of two monitoring points were required.

Families of type curves were generated for different well pair spacing and orientations of fracture planes and a high pulse pressure response impact was evidenced between the pulse well and monitoring points.

To evaluate this technique in a field scale condition, a field data validation was conducted. Inversion techniques were applied to match the numerical results with the field observations. A reasonable match for fracture height and orientation was determined. Even though the conceptual model was designed for tight gas reservoirs, this technique can be implemented for a range of field conditions including conventional and unconventional reservoirs.

Further research on this topic is ongoing to characterize multi stage hydraulic fractures using pressure pulse test analysis.

REFERENCES

Ahmed, T. and McKinney, P. 2005. *Advanced reservoir engineering*. 1st ed. Oxford: Elsevier.

Brigham, W. E. 1969. Planning and analysis of pulse-tests. In *Proceedings of the SPE Improved Oil Recovery Symposium, Tulsa, Oklahoma, 13 – 15 April, 1969.* SPE 2417.

Cinco-Ley, H., and V. F. Samaniego. 1977. Determination of the orientation of a finite conductivity vertical fracture by transient pressure analysis. In *Proceedings of the 1977 SPE Annual Technical Conference and Exhibition, Denver, Colorado, 9-12 October, 1977.* SPE 6750.

Earlougher R. C. 1979. Analysis and design methods for vertical well testing. In *Proceedings of the SPE 54th Annual Fall Technical Conference and Exhibition, Las Vegas, 23-26 September, 1979.* SPE 8038.

Ekie, S., N. Hadinoto, and R. Raghavan. 1977. Pulse-testing of vertically fractured wells. In *Proceedings of the SPE* Annual *Technical Conference and Exhibition, Denver, 9–12 October, 1977.* SPE 6751.

El-Khatib, N. 2011. Design and analysis of single pulse tests. *Journal of Petroleum Science and Engineering.* 77:69-77.

El-Khatib. 2013. New approach for pulse test analysis. In *Proceedings of the SPE North Africa Technical Conference and Exhibition, Cairo, Egypt, 15-17 April, 2013.* SPE 164597.

Gringarten, A. C., H. J. Ramey, and R. Raghavan. 1972. Unsteady-state pressure distributions created by a well with a single infinite-conductivity vertical fracture. In *Proceedings of the SPE-AIME 47th Annual Fall Meeting, San Antonio, Texas, 8-11 October, 1972.* SPE 4051.

Johnson, C. R., R.A. Greenkorn, and E.G. Woods. 1966. Pulse testing: a new method for describing reservoir flow properties between wells In *Proceedings of the SPE 41st Annual Fall Meeting, Dallas, Texas, 2-5 October, 1966.* SPE 1517.

Kamal, M. and W.E., Brigham. 1974. Design and analysis of pulse tests with unequal pulse and shut-in periods. In *Proceedings of the SPE-AIME 44th Annual California Regional Meeting, San Francisco, California, 4-5 April, 1974.* SPE 4889.

Kamal M.M. 1982. Interference and pulse testing – a review. In *Proceedings of the 1982 SPE International Petroleum Exhibition and Technical Symposium, Beijing, China, 18-26 March, 1982.* SPE 10042.

Lawrence Berkeley National Laboratory. 2012. TOUGH2 user's guide, version 2. California. LBNL-43134.

Pierce, A.E., S. Vela, and K.T. Koonce. 1974. Determination of the compass orientation and length of hydraulic fractures by pulse testing. In *Proceedings of the SPE-AIME 49th Annual Fall Meeting, Houston, Texas, 6-9 October, 1974.* SPE 5132.

Uraiet, A., R. Raghavan, and G. W. Thomas. 1977. Determination of the orientation of a vertical fracture by interference tests. *Journal of Petroleum Technology*. 29:73-80.

Vela, S. and R.M. McKinley. 1969. How areal heterogeneities affect pulse-test results. In *Proceedings of the SPE 44th Annual Fall Meeting, Denver, Colorado, 28 Septiembre – 1 Octubre, 1969.* SPE 2569.

World Stress Map. 2016. Retrieved from: http://www.world-stress-map.org/.